Unified Modeling of PWM Converters With Regular or Tapped Inductors Using TIS-SFG Approach

Alexander Abramovitz, Jia Yao, and Keyue Smedley

***Abstract*—This paper revisits the switched flow graph (SFG) technique. A general and unified equivalent SFG model of a three-terminal switcher encountered in regular and tapped inductor converters operating in the continuous conduction mode is proposed. The model can be applied to most PWM topologies and facilitates construction of a complete flow graph of a given converter. The approach can be helpful in theoretical analysis and derivation of analytical expressions of converter's small-signal transfer functions. The suggested methodology extends the previously proposed SFG analysis technique and alleviates the principal difficulties involved. Furthermore, the approach is straightforward and expeditious. Application guidelines and examples are presented and compared to simulation and earlier theoretical results.**

***Index Terms*—Averaged modeling, feedback, feedback circuits, switch-mode power conversion.**

I. Introduction

DYNAMIC modeling is a forestay of stability analysis and control loop design of switch-mode power converters. The challenges in modeling of the switched power stages are twofold. The primary task is modeling the switcher [1], whereas the second is modeling the PWM modulator function [2]–[4]. The rest of the controller circuitry, mainly the analog error amplifier, easily lends itself to modeling by the familiar operational amplifier analysis techniques and requires no special consideration.

In the past, several theoretical approaches were proposed to describe the dynamic behavior of PWM power stages [1]–[5]. One of the earliest developments was the averaged circuit approach [6] and the state-space averaging [1]–[7], [8], which established the foundation for switching converter dynamic modeling. Many methods followed, such as the Canonical model [1], [9], [10]; the current injected control approach [11], [12]; the sampled data model [13]–[15]; switching flow graph (SFG) [16]; the switched inductor model [17]–[19]; Y-parameters approach [20]; and the PWM switch model [21]. These techniques differ by their derivation and application approach; however, each one can be applied to obtain the small-signal transfer functions of a given PWM converter.

The SFG technique [16] is a general graphic nonlinear modeling tool and an extension to the linear circuit signal flow graph theory that can provide visual representation of a switching converter. The SFG utilizes the state-space averaging concept [8], but has extended capability of predicting large-signal behavior in addition to steady state and small signal ones, suitable for dynamic modeling of switched-mode converters and inverters where large dynamic range is expected [30]–[37]. Furthermore, with SFG, the analytic relationship between any two variables on the graph, i.e., the desired transfer function, can be obtained applying the familiar block diagram algebra or Mason's rule. The resulting small-signal transfer functions are identical to those derived by the state-space averaging method, but large-signal model and arbitrary point-to-point analytic transfer functions are additional merits. Possibly, most modeling problems of the switched power stages can be handled by the already established state space or switch model methods; thus, the motivation for using SFG did not become overwhelming.

Recent developments in the renewable sector have stimulated new interest in high-gain power converter study and a considerable number of new converters were proposed based on the tapped inductor (TI) concept. It becomes relatively more difficult to obtain accurate dynamic models for this group of converters due to many possible variations of tap connections and taking the correct account of the coupling phenomenon. In fact, the incentive for this study was the recently published [23], which discussed the topological aspects of TI family. Tapped/coupled inductor converters can be derived from the standard buck, boost, and buck–boost topologies and constitute a class of converters with extended conversion ratio range. These converters can achieve higher step up or step down ratios at moderate duty cycle and are advantageous in certain applications including renewable integration. The subject of the dynamic modeling of the TI converters is of a fundamental importance for supporting such applications. The TI converters are more complicated compared to their nontapped counterparts. For this reason, the number of publications dealing specifically with the intricacies of dynamic modeling of TI converters is limited and no general approach was presented so far. Yet, the application potential and high visibility of TI converters certainly warrant them for deeper consideration.

This paper suggests a generalized treatise of the dynamics of the TI converters based on the SFG technique. The presented idea is hinged on the fact that most PWM converters utilize a switched inductive device either simple or coupled. Such a switcher can be regarded as an invariant building block of PWM converters [6]. The switcher is a nonlinear and time-varying network and, hence, presents the primary modeling challenge. The rest of the power stage, i.e., the input and the output filters, constitute a linear circuit. Therefore, once derived, the switcher

Manuscript received November 7, 2014; revised February 7, 2015; accepted April 2, 2015. Date of publication April 28, 2015; date of current version September 29, 2015. Recommended for publication by Associate Editor M. Ordonez.

The authors are with the Department of Electrical Engineering and Computer Science, University of California, Irvine, CA 84100 USA (e-mail: alabr@hotmail.com; seu.yaojia@gmail.com; smedley@uci.edu).

Color versions of one or more of the figures in this paper are available online at http://ieeexplore.ieee.org.

Digital Object Identifier 10.1109/TPEL.2015.2424255

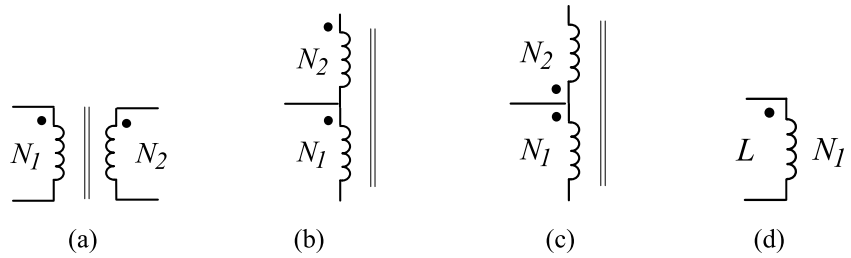

Fig. 1. Common inductive elements: (a) isolated coupled inductors (flyback transformer); (b) cumulatively wound TI; (c) differentially wound TI; (d) regular inductor.

equivalent subgraph model can be embedded into the flow graph of the problem converter regardless of its topology and help obtaining a complete SFG model of any PWM converter. The presented equivalent SFG subgraph is just one possible embodiment of the model. Other modeling methods, like state-space or averaged circuit approaches could have been considered to construct the model. However, the graphical nature of the SFG method is of a great advantage since it allows regarding the proposed model as a subgraph to be used similarly to application of equivalent circuits in network analysis. The required small-signal transfer functions can be found applying either signal flow graph algebra or Mason's rule, whereas complex graphs can be solved using general purpose computational software packages like MATLAB, MAPLE, MATHEMATICA, etc.

II. TI Switcher

A. Preliminary Considerations

Inductive energy transfer is a basic concept of PWM converters. This class of converters relies on charging an inductor from the input voltage source and discharging it to the output. In order to extend the voltage conversion range, some PWM topologies use coupled inductors. Though coupled inductors with multiple winding are feasible, in practice, the two winding-coupled-inductor structure is the most commonly used. Depends on the interconnect pattern, coupled inductors can be either isolated or nonisolated. The nonisolated coupled inductors, also referred to as TIs, can be configured with either cumulative or differential winding arrangement. The dot convention is conveniently used to identify positive polarity of winding voltages. Common inductive elements used in power electronics are shown in Fig. 1.

To implement the inductor charging and discharging, a suitable switching arrangement is needed. The simple switch is realized with one active and one passive semiconductor devices, whereas synchronous or bidirectional converters use two or more active devices. For instance, the three basic PWM buck, boost, and buck–boost converter topologies [see Table I(a)–(c)], can be created by rotating the switcher and adjusting the polarity of the semiconductors to suit the current polarity [6], [22]. Some of the TI counterparts can be created similarly; however, TI constitutes a more complex case and, therefore, additional considerations apply. Derivation procedure of TI topologies can be found in [23]. TI converters can be classified according to winding arrangement and tap connection [23], [24]–[26]. Three major options are switch-to-tap, diode-to-tap, and rail-to-tap. Input, output, or ground rails can be identified. A list of selected TI converters is given in Table I. TIs with cumulative windings may have somewhat reduced volume compared to the differentially wound TIs. For this reason, converters with cumulative TIs are more popular than with the differential arrangement.

B. Derivation of the TIS Model

The proposed tapped inductor switcher (TIS), illustrated in Fig. 2, is an invariant building block of most TI PWM converters. TIS can be identified as a part of the TI topologies, as illustrated in Table I. The difference in between the TI topologies and accordingly, their voltage converter ratio, is in the way the TIS block is embedded in the converter topology. The rules of determining the parameters of the TIS model are discussed next.

1) TIS Terminals: The voltage sources V_0, V_1, V_2 in Fig. 2 represent the voltages imposed on TIS by the rest of the circuit. It is assumed that the switch on terminal 1 is the active switch controlled by the $K\,(d)$ switching signal, whereas the switch on terminal 2 is either passive or a complimentary active switch activated by the complimentary $K'\,(d')$ switching signal.

2) TIS Effective Number of Turns: The effective number of turns seen between terminal 1 and 0 upon activation of $K\,(d)$ switch is defined as N_{10}, whereas the effective number of turns seen between terminal 2 and 0 upon activation of $K'\,(d')$ switch is defined as N_{20}. Depends on the converter's topology and windings arrangement, the effective number of turns N_{10} and N_{20} are functions of TI's original N_1 and N_2 number of turns and interconnect and can be either positive or negative. Therefore, winding identification and polarity deserve attention. The N_1 winding in the *original* topology (see Table I) is identified as the one used for charging the TI and adjacent to the active switch Q. Positive polarity of N_1 winding is designated by a dot placed on its switched terminal and serves as a reference. The polarity of N_2 winding is determined by the topology and can be arbitrary. Accordingly, the positive sense of N_{10} and of N_{20} windings in the TIS model corresponds to the positive polarity of N_1 and is designated by the dot convention as illustrated in Fig. 2.

3) TIS Magnetizing Inductance: The magnetizing inductance L_m in Fig. 2 is associated with the N_{10} winding and is given by

$$L_m = L_1 \left(\frac{N_{10}}{N_1}\right)^2 \tag{1}$$

TABLE I
LIST OF SELECTED TI CONVERTERS AND THEIR ASSOCIATED WINDING RATIO, a.

		Buck	Boost	Buck-Boost
Standard		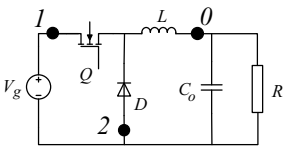 $a=1$ (a)	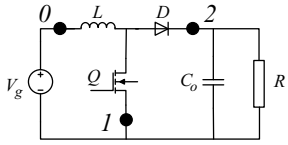 $a=1$ (b)	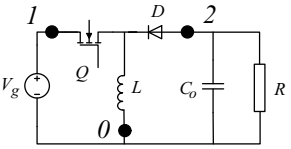 $a=1$ (c)
Cumulative windings	Switch to tap	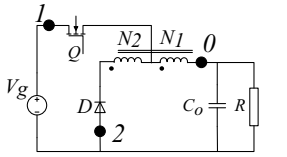 $a=1/(1+n)$ (d)	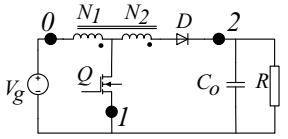 $a=1/(1+n)$ (e)	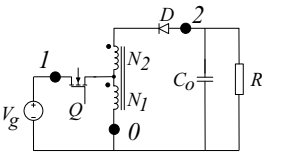 $a=1/(1+n)$ (f)
	Diode to tap	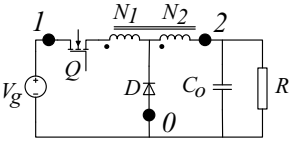 $a=1+1/n$ (g)	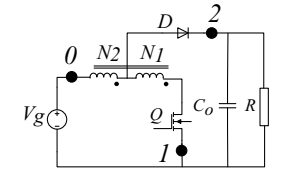 $a=1+1/n$ (h)	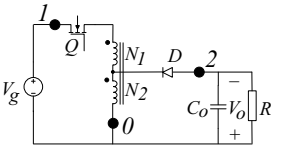 $a=1+1/n$ (i)
	Rail to tap	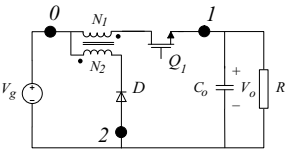 $a=-1/n$ (j)	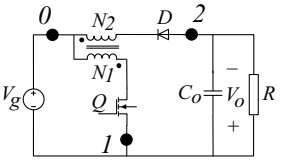 $a=-1/n$ (k)	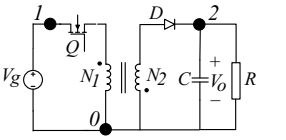 $a=-1/n$ (l)
Differential windings	Switch to tap	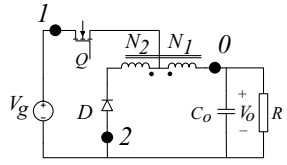 $N_1>N_2$ $a=1/(1-n)$ (m)	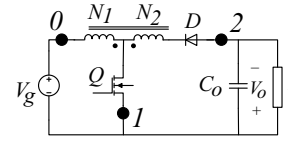 $N_1<N_2$ $a=1/(1-n)$ (n)	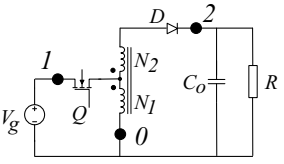 $N_1<N_2$ $a=1/(1-n)$ (o)
	Diode to tap	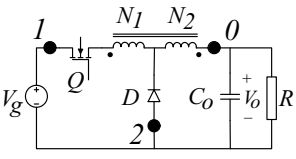 $N_1<N_2$ $a=1-1/n$ (p)	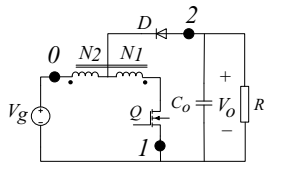 $N_1>N_2$ $a=1-1/n$ (q)	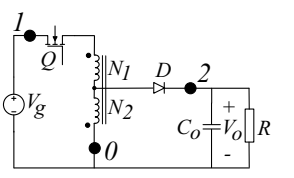 $N_1>N_2$ $a=1-1/n$ (r)
	Rail to tap	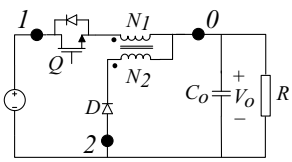 $a=1/n$ (s)	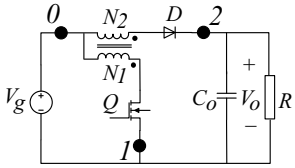 $a=1/n$ (t)	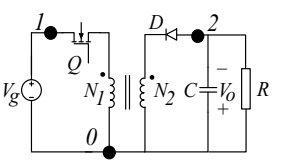 $a=1/n$ (u)

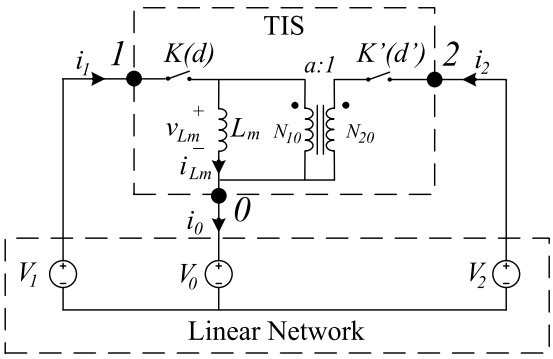

Fig. 2. TIS—a common building block of TI and PWM converters.

where L_1 is the inductance of the original N_1 winding, measured with N_2 winding opened (leakage neglected).

4) TIS Effective Winding Ratio: As usual, the *turn ratio n* is defined as the ratio of the *original* TI's number of turns N_1 and N_2

$$\boldsymbol{n} = \frac{\boldsymbol{N_2}}{\boldsymbol{N_1}} \tag{2}$$

Henceforth, a parameter, referred to as the *effective winding ratio a* is introduced as the ratio of the *effective* number of turns N_{10}, and N_{20}

$$\boldsymbol{a} = \frac{\boldsymbol{N_{10}}}{\boldsymbol{N_{20}}}. \tag{3}$$

Depending on converter topology and TI's winding arrangement, four cases can be identified as follows:

1) Direct charging or discharging (through a *single* winding), here $N_{10} = N_1$ or $N_{20} = \pm N_2$, respectively. For instance, the coupled inductor of the flyback converter in Table I(l) charges only through the primary and discharges only through the secondary winding. Hence, $N_{10} = N_1$ and $N_{20} = -N_2$, considering the negative sense of the secondary winding with regard to Fig. 2. Therefore, the winding ratio of flyback converter is

$$a = \frac{N_1}{-N_2} = -\frac{1}{n}. \tag{4}$$

2) Augmenting charging or discharging (through both windings connected in series with *same polarity*) here $N_{10} = N_1 + N_2$ or $N_{20} = N_1 + N_2$, respectively. For instance, the cumulatively wound TI-boost converter in Table I(e) accomplishes charging through the primary winding, hence $N_{10} = N_1$, whereas discharge occurs through both windings in series with the secondary winding aiding the primary so that $N_{20} = N_1 + N_2$. Therefore, the effective winding ratio is

$$\boldsymbol{a} = \frac{\boldsymbol{N_1}}{\boldsymbol{N_1 + N_2}} = \frac{\boldsymbol{1}}{\boldsymbol{1 + n}}. \tag{5}$$

The cumulatively wound TI buck converter in Table I(g) is charged through aiding series windings so that $N_{10} = N_1 + N_2$, and discharges through secondary only, hence $N_{20} = N_2$. Therefore, the effective winding ratio is

$$\boldsymbol{a} = \frac{\boldsymbol{N_1 + N_2}}{\boldsymbol{N_2}} = \boldsymbol{1} + \frac{\boldsymbol{1}}{\boldsymbol{n}} \tag{6}$$

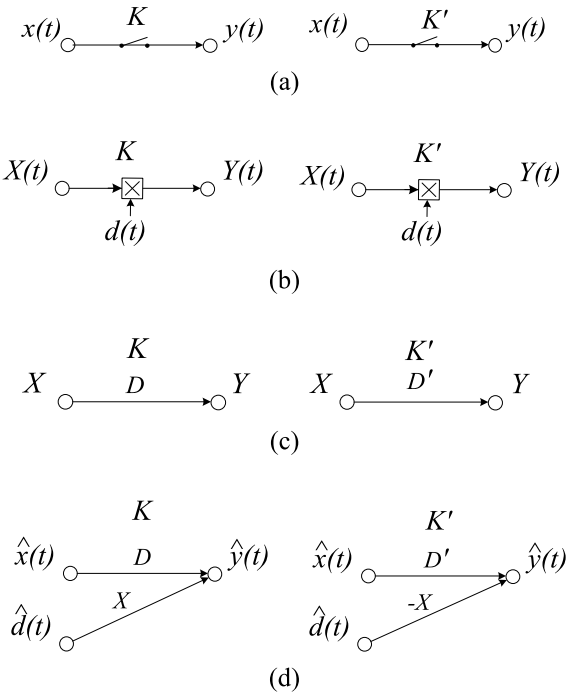

Fig. 3. Derivation of switched branch models [16]: (a) switched branch; (b) large-signal model of the switched branch; (c) steady-state model of the switched branch; (d) small-signal dynamic model of the switched branch.

3) Counteracting charging or discharging (through windings connected in series with opposing polarity), here $N_{10} = N_1 - N_2$ or $N_{20} = N_1 - N_2$, respectively. For instance, the differentially wound TI buck converter in Table I(m), charges the TI through its primary winding so $N_{10} = N_1$. TI is discharged through both windings in series with the secondary winding in opposition to the primary; therefore, $N_{20} = N_1 - N_2$. The resulting winding ratio is

$$\boldsymbol{a} = \frac{\boldsymbol{N_1}}{\boldsymbol{N_1 - N_2}} = \frac{\boldsymbol{1}}{\boldsymbol{1 - n}}. \tag{7}$$

4) Trivial case: A regular inductor can be regarded as a particular case of a nonisolated TI with $N_2 = 0$. Thus, the winding ratio for of the PWM converters listed in Table I(a–c) equals unity

$$\boldsymbol{a} = \frac{\mathbf{N_1}}{\boldsymbol{N_1}} = \boldsymbol{1}. \tag{8}$$

Hence, (3) can yield the effective winding ratio a, either smaller or greater than unity, and with either positive or negative sign. Negative a manifests polarity reversal of the terminal 2 current and, consequently, voltage. The winding ratio a of the selected TI converters is given in Table I.

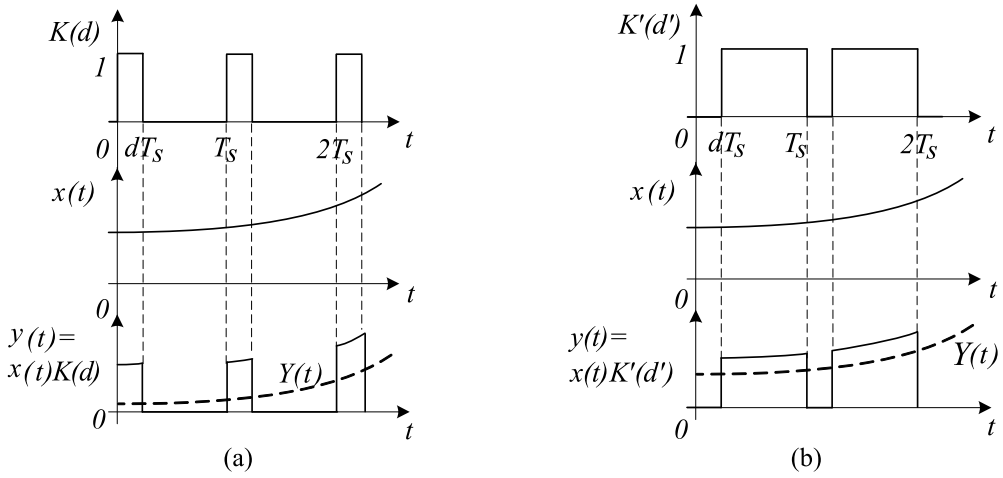

Fig. 4. Waveforms of the switched branches: (a) $K(d)$ switched; (b) $K'(d')$ switched. Upper trace: the switching function $K(d)$; middle trace: the input signal $x(t)$; lower trace: the instantaneous (chopped) output signal $y(t)$ and its time varying average $Y(t)$.

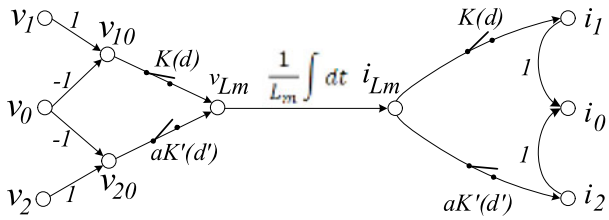

Fig. 5. SFG of ideal TIS.

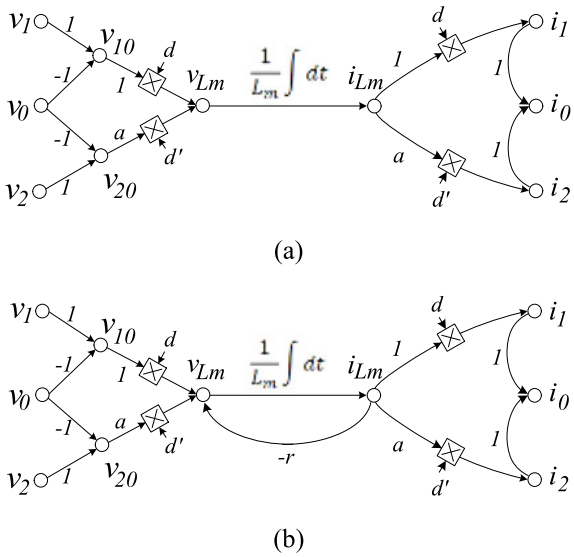

Fig. 6. Large-signal (average) SFG models of a TIS: (a) ideal case; (b) non-ideal case, including the equivalent resistance, r.

III. Quick Reference to SFG Modeling Method

To begin with, a brief introduction to the SFG modeling approach [16] is given.

The switched converters such as pulse-width-modulated (PWM) converters are nonlinear dynamic systems. However, in the *continuous conduction mode* (*CCM*), during switch ON and OFF intervals, their state can be represented by linear equivalent circuits and, correspondingly, by linear signal flow graphs. Comparison of the ON and OFF flow graphs reveals that some branches that exist in the ON flow graph do not exist in the OFF flow graph and vice versa. These branches are referred to as the switched branches and a graph containing the switched branch is referred to as the SFG. The switched branches are the only nonlinear components of SFG. The symbol of the switched branch is shown in Fig. 3(a). The function of a switched branch can be either established or broken depends on the value of the switching function *K(d(t))* defined by

$$K(d(t)) = \begin{cases} 1, & 0 \le t < dT_s \\ 0, & dT_s \le t < T_s \end{cases} \tag{9}$$

or, alternatively, by the complementary switching function $K'(d'(t))$ defined by

$$K'(d'(t)) = \begin{cases} 0, & 0 \le t < dT_s \\ 1, & dT_s \le t < T_s. \end{cases} \tag{10}$$

Based on the state-space averaging concept, the switched branch model can be linearized as shown in Fig. 3. Examining the signals of the switched branch in Fig. 3(a), the *averaged over a switching cycle* output signal $y(t)$ carried at the output of the and $K(d(t))$ branch can be derived as the product of the input signal $x(t)$ and the duty-ratio control signal $d(t)$: $y(t) = d(t)x(t)$. Therefore, the averaged large-signal model of a switched branched can be represented by a multiplier as illustrated in Fig. 3(b). For steady-state case, where the signals and duty-ratio control signals $x(t)$, $y(t)$, $d(t)$ assume constant values *X, Y,* and *D* respectively. Here, the branch steady-state output is $Y = DX$. Hence, the switched branch model in Fig. 3(b) can be simplified and yields the steady-state switched branch model, as shown in Fig. 3(c), where the duty ratio *D* appears as the gain of the branch.

Furthermore, for the small-signal model of the switched branch, introducing small-signal perturbations $\hat{x}(t)$, $\hat{y}(t)$, and

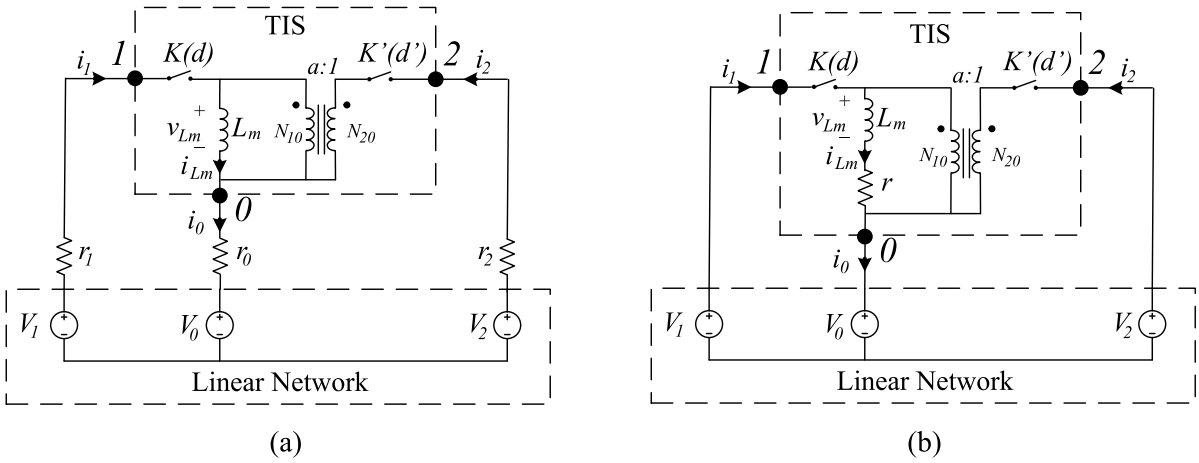

Fig. 7. Practical TIS: (a) considering terminal resistances; and (b) with an equivalent resistance.

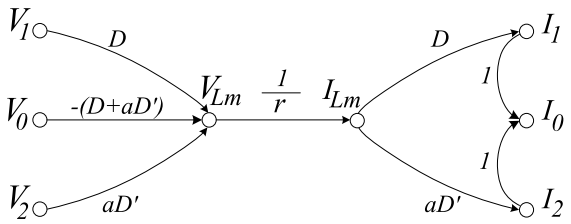

Fig. 8. Steady-state TIS-SFG model.

$\hat{d}(t)$ near the operating point X, Y, D, the signal carried at the output of the switched branch is $Y + \hat{y}(t) = (D + \hat{d}(t))(X + \hat{x}(t))$. Neglecting the steady-state solution and the second-order terms, the small-signal output perturbation can be approximated to $\hat{y}(t) \approx X\hat{d}(t) + D\hat{x}(t)$. The resulting small-signal switched branch model is shown in Fig. 3(d). Note that the operating point data *X* and *D* appear as gain of the corresponding branch.

The models for $K'(d'(t))$ branch can be derived similarly; however, here, the sign reversal has to be considered due to $\widehat{d'} = -\hat{d}$ relationship (CCM assumed).

To apply the earlier SFG analysis procedure: 1) draw the SFGs of the ON and OFF states, 2) identify the switched branches and their switching functions, and 3) merge the ON and OFF graphs to attain the SFG model, 4) apply the appropriate branch model (steady-state model for dc analysis and the small-signal model for dynamic analysis). Application of the linearized models of switched branches in Fig. 3 yields the graphical linearized SFG model of the switched converter under study [16]. The concluding step in the dynamic analysis is 5) derivation of the desired dc relationships or transfer functions.

The earlier SFG analysis method is somewhat time and effort consuming since it involves dealing with switched branches—an idea unfamiliar to most. An expeditious approach proposed in this paper is based on using a "prefabricated" generalized TIS-SFG subgraph, which can be applied as an equivalent circuit. So that a complete SFG model of a switching converter can be obtained by a proper substitution of the equivalent TIS-SFG subgraph. Since TIS-SFG subgraph already includes all the switched branches, the modeling effort is greatly reduced. Moreover, since the equivalent TIS-SFG can represent switchers incorporating both regular and coupled inductors, the proposed approach is applicable to a wide variety of PWM converters.

IV. Derivation of the SFG Models of the TIS

A. SFG Model of an Ideal TIS

In CCM, the TIS in Fig. 2 can have two topological states. During the ON state, the switching function *K(d(t))* assumes its active value and establishes its branch function, whereas the complementary switching function $K'(d'(t))$ deactivates and breaks (nulls) its branch function. Hence, the voltage across the magnetizing inductance v_{Lm} is the voltage difference $v_{10} = (v_1 - v_0)$. During the OFF state, the function $K(d(t))$ deactivates and breaks its branch function, while the complementary switching function $K'(d')$ assumes its active value and establishes its branch function. Considering the winding ratio *a* of the TI (see (8)), the voltage across the magnetizing inductance v_{Lm} equals $av_{20} = a(v_2 - v_0)$. Therefore, the instantaneous magnetizing inductor voltage can be written in a generalized form as follows:

$$v_{Lm}(t) = K(d(t))v_{10}(t) + aK'(d'(t))v_{20}(t). \quad (11)$$

With regard to Fig. 2, the current of terminal 1 i_1 flows when the switching function *K(d(t))* is activated

$$i_1(t) = K(d(t))\, i_{Lm}(t). \quad (12)$$

Similarly, the current of terminal 2 i_2 appears when the complementary switching function $K'(d'(t))$ is active

$$i_2 = aK'(d(t))\, i_{Lm}. \quad (13)$$

By Kirchhoff's law, the current of the common terminal 0 i_0 is

$$i_0(t) = i_1(t) + i_2(t). \quad (14)$$

The SFG model of an ideal TI representing (11)–(14) can be constructed, as shown in Fig. 5. The graph describes the

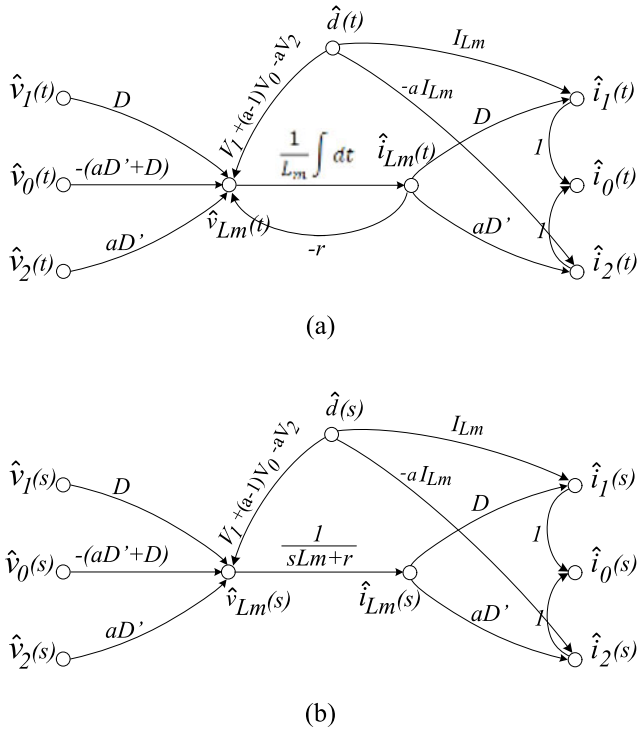

Fig. 9. Small-signal TIS-SFG model in: (a) time domain; (b) frequency domain.

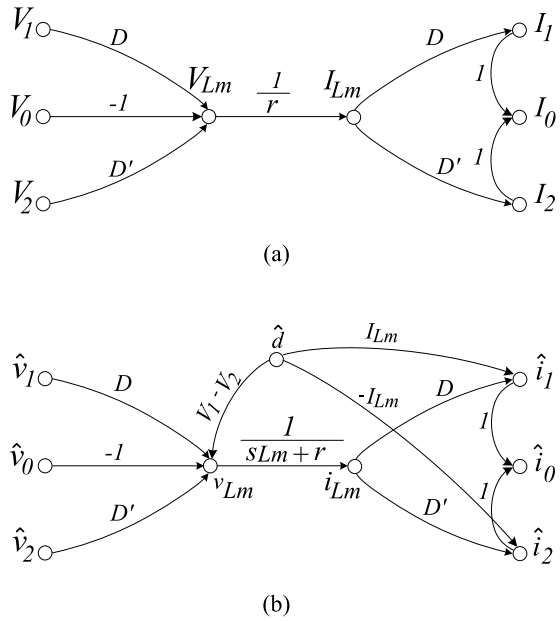

Fig. 10. SFG models of a switched inductor: (a) steady state; (b) small-signal frequency domain.

relationships between the instantaneous variables; however, in sake of brevity, here, the time variable *t* is omitted.

B. Large-Signal TIS-SFG Model

From Section III above, the *average* large-signal model of the ideal TIS can be obtained replacing the switched branches by multipliers, as illustrated in Fig. 6(a). Here, the control variables d and d' at the multipliers' inputs are allocated according to the nature of the switching functions $K(D)$ and $K'(D')$, respectively.

The losses of the nonideal TIS can be modeled adding a feedback branch $-r$ around the integrator branch $\frac{1}{L_m}\int^d t$, as shown in Fig. 6(b). The equivalent resistance of the TIS *r* is evaluated next.

C. Considering the Losses of a Nonideal TIS

A practical nonideal TIS has a resistance on each of its terminals, as shown in Fig. 7(a). The origin of these components is briefly described in the appendix. Though fairly small, the voltage drops across the parasitic resistances to modify the magnetizing voltage. An easy way to realize the effect of parasitic resistances is to consider the volt–sec balance of the magnetizing inductor in the steady state. Obviously, in presence of the terminal resistances r_0, r_1, and r_2, the *average* voltage across the magnetizing inductance $< v_{Lm} >$ is not only a function of terminal voltages V_0, V_1, V_2 but also of the *terminal* currents i_1, i_2

$$\begin{aligned} < v_{Lm} > \; = \; 0 = D\left[(V_1 - V_0) - (r_0 + r_1)i_1\right] \\ + aD'\left[(V_2 - V_0) - (r_0 + r_2)i_2\right]. \end{aligned} \quad (15)$$

Recall that during the ON interval DTs, $i_1 = i_{Lm}$, whereas during the OFF interval $D'Ts$, $i_2 = ai_{Lm}$; therefore, (15) can be rewritten as a function of the terminal voltages and the *magnetizing* current i_{Lm}

$$\begin{aligned} < v_{Lm} > = 0 = \; & D\left(V_1 - V_0\right) + aD'\left(V_2 - V_0\right) - \left[D\left(r_0 + r_1\right)\right. \\ & \left. + a^2 D'\left(r_0 + r_2\right)\right] i_{Lm} \\ = \; & D\left(V_1 - V_0\right) + aD'\left(V_2 - V_0\right) - r i_{Lm}. \end{aligned} \quad (16)$$

Equation (16) suggests that the effect of parasitic resistances in Fig. 7(a) can be modeled by a single equivalent resistance *r*, which appears in *series with the magnetizing inductance* L_m, as shown in Fig. 7(b) and is given by

$$r = D\left(r_0 + r_1\right) + a^2 D'\left(r_0 + r_2\right). \quad (17)$$

The equivalent resistance *r* can be easily incorporated into the SFG model, as illustrated in Fig. 6(b).

D. Steady-State TIS-SFG Model

From Section III above, to attain the steady-state average model of the TIS, the multipliers in Fig. 6 are simply replaced by the averaged branches, whose gain equals the average value of the duty cycles D and D', respectively. Thus, the average steady-state SFG model of TIS arises as in Fig. 8. Here, some additional manipulation was performed to reveal the branch connecting V_0 and V_{Lm}. Under the steady-state conditions, it is assumed that the signals at all the input and output terminals of

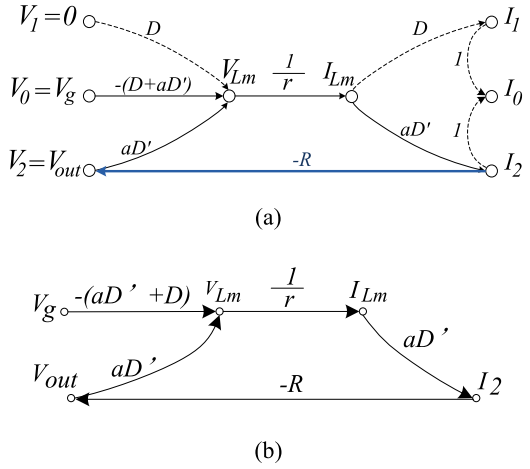

Fig. 11. Steady-state TIS-SFG models of TI boost: (a) initial and (b) simplified.

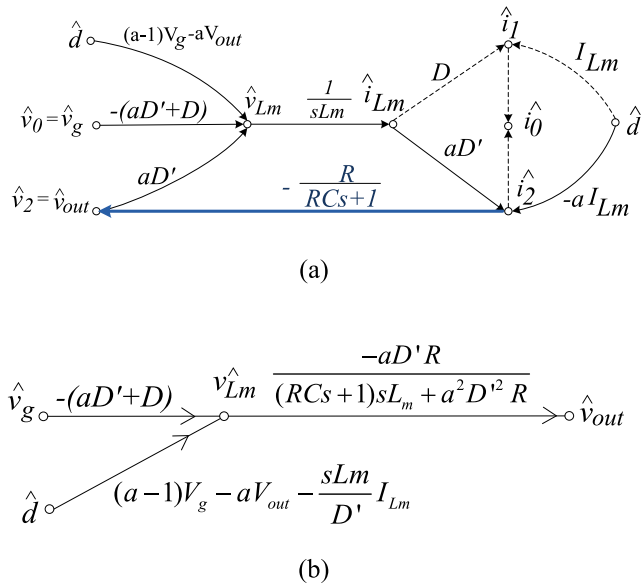

Fig. 12. Small-signal SFG model of TI boost: (a) initial model and (b) simplified small-signal SFG model.

the SFG are the dc values

$$\begin{cases} v_0(t) = V_0 \\ v_1(t) = V_1 \\ v_2(t) = V_2 \\ i_0(t) = I_0 \\ i_1(t) = I_1 \\ i_2(t) = I_2. \end{cases} \tag{18}$$

Hence, the steady-state average SFG model in Fig. 8 represents the dc relationships. The proposed model is invariant and can be applied as is to most PWM topologies. The model can be used to obtain the analytical dc solution of converter voltages and currents as a function of the duty cycle *D*, and the TI winding ratio *a*.

The steady-state TIS-SFG model in Fig. 8 correctly reflects the volt–sec balance of the magnetizing inductor. Since the converter operates with finite average magnetizing current I_{Lm}, for low *r*, the infinite dc gain of the *1/r* path implies that under steady-state conditions, the average magnetizing inductor voltage V_{Lm} vanishes

$$V_{Lm} = D(V_1 - V_0) + aD'(V_2 - V_0) = \lim_{r\to 0} rI_{Lm} = 0. \tag{19}$$

This stands in accord with the established theory of analysis of switching converters.

E. Small-Signal TIS-SFG Model

To derive the small-signal model of the TIS, the multipliers in Fig. 6 are substituted by appropriate small-signal subgraphs as discussed in Section III above. The gain of the branches is determined by the dc values of the appropriate variables. Applying the usual $\hat{d}' = -\hat{d}$ further simplification yields the small-signal average SFG models are shown in Fig. 9(a).

The small-signal average SFG model in Fig. 9 can be considered as a subgraph, invariant of the converter topology, and can be applied in dynamic analysis of PWM converters (see Fig. 9). This dynamic model considers only the small-signal perturbations at its input and output terminals

$$\begin{cases} v_0(t) = \hat{v}_0(t) \\ v_1(t) = \hat{v}_1(t) \\ v_2(t) = \hat{v}_2(t) \\ i_0(t) = \hat{i}_0(t) \\ i_1(t) = \hat{i}_1(t) \\ i_2(t) = \hat{i}_2(t). \end{cases} \tag{20}$$

The effect of parasitic resistances requires additional attention and is discussed next.

Introducing the small-signal perturbations into (16) gives

$$\begin{aligned} \hat{v}_{Lm} = {} & D\hat{v}_{10} + aD'\hat{v}_{20} - \left[D(r_0 + r_1) + a^2 D'(r_0 + r_2)\right]\hat{i}_{Lm} \\ & + (V_{10} - V_{20})\hat{d} - \left[(r_0 + r_1) - a^2(r_0 + r_2)\right] \\ I_{Lm}\hat{d} = {} & D\hat{v}_{10} + aD'\hat{v}_{20} - r\hat{i}_{lm} - [(V_{10} - (r_0 + r_1)I_{Lm}) \\ & -(V_{20} - a^2(r_0 + r_2)I_{Lm})]\hat{d} \end{aligned} \tag{21}$$

here the coefficient of $\hat{i}_{Lm}$ is identical to (17) and, therefore, is identified as the equivalent resistance *r*.

Efficiency considerations can help appreciating the coefficients of $\hat{d}$ in (21). Here, V_{10} is the voltage across the primary winding and $(r_0 + r_1) I_{Lm}$ is the voltage drop across the parasitic resistances during DT_S interval. To attain good efficiency, the converter should be designed so that $V_{10} \gg (r_0 + r_1) I_{Lm}$. Similar considerations apply to the *D'Ts* interval, where V_{20} is the voltage across the series connection of primary and secondary windings and $a^2 (r_0 + r_2) I_{Lm}$ is the voltage drop across the parasitic resistances during *D'Ts* interval. Again, proper converter design requires $V_{20} \gg a^2 (r_0 + r_2) I_{Lm}$. Furthermore,

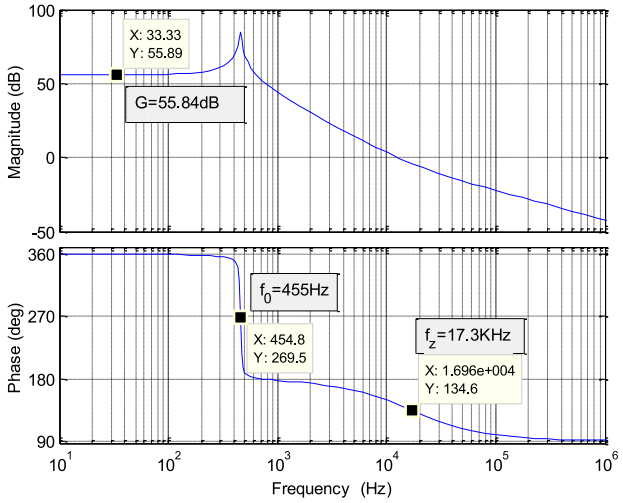

Fig. 13. Control-to-output frequency response plot of TI-boost converter ($D = 0.56$, $N = 2$, $R_{\rm load} = 200\ \Omega$, $V_O = 200$ V, $V_g = 40$ V, $L_m = 56\ \mu$f, $C_o = 47\ \mu$f, $f_{\rm S} = 50$ kHz).

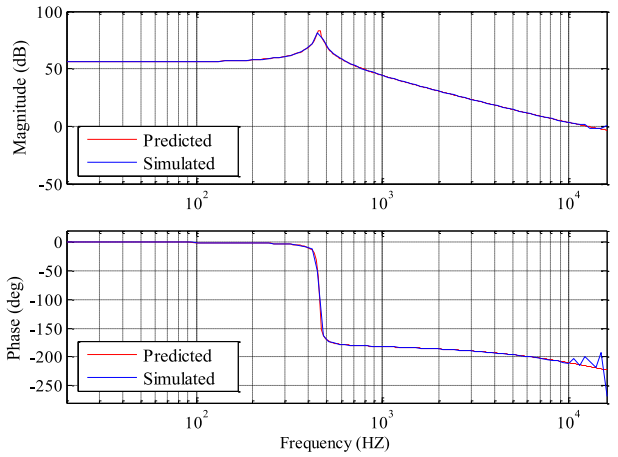

Fig. 14. Comparison of the calculated versus simulated control-to-output frequency response $\hat{v}_{\rm out}/\hat{d}$ of cumulatively wound TI-boost converter ($D = 0.56$, $N = 2$, $R_{\rm load} = 200\ \Omega$, $V_O = 200$ V, $V_g = 40$ V, $L_m = 504\ \mu$f, $C_o = 47\ \mu$f, $f_S = 50$ kHz).

to satisfy volt–sec balance of magnetizing inductance $L_{\rm m}$ (see (11)), the voltages V_{10} and V_{20} must have opposing signs; therefore, the difference term $V_{10} - V_{20} = \pm(|V_{10}| + |V_{20}|)$ ever vanishes and is much larger than the last term in (21). These considerations justify the approximation

$$\hat{v}_{Lm} = D\hat{v}_{10} + aD'\hat{v}_{20} - r\hat{i}_{Lm} + (V_{10} - V_{20})\,\hat{d}. \qquad (22)$$

Therefore, according to (22), the effect of parasitic resistances on small-signal model of TIS can be represented by identical equivalent resistance *r*, similarly to the steady-state case.

Hitherto, the discussion was conducted in the time domain. In order to conduct dynamic analysis of PWM converters and obtain the desired transfer functions, the derived TIS small-signal model is translated to the frequency domain, as shown in Fig. 9(b). The parameters required by the small-signal TIS-SFG model are the TI primary winding magnetizing inductance

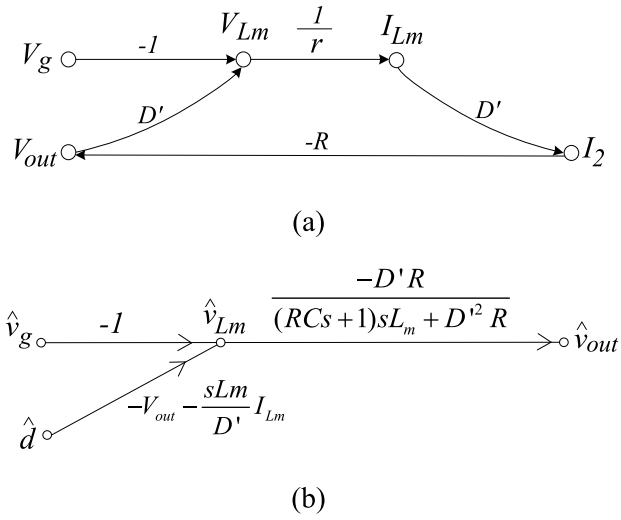

Fig. 15. SFG models of the basic boost PWM converter derived from TI boost applying $a = 1$ condition: (a) steady-state SFG; (b) small-signal SFG.

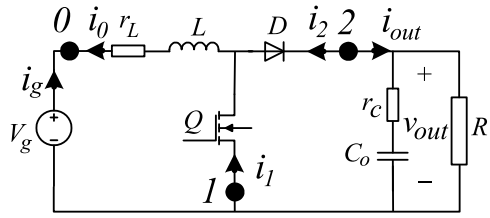

Fig. 16. Boost converter including parasitic resistances r_L and r_C.

L_m, its winding ratio *a*, as defined by (3)–(8), and the dc operating point data. These can be obtained from the steady-state SFG model described above and considering the details of the topology at hand.

F. Corollary: Modeling the PWM Converters

Traditional PWM converters, such as shown in Table I(a), (b), and (c), operate with a regular inductor. As mentioned above, see (8), a regular inductor can be regarded as a trivial case of the TI. Therefore, the SFG models in Figs. 8 and 9 can be reduced to cover the case of the simple switched inductor. This can be obtained by direct substitution of $a = 1$ into Figs. 8 and 9. Further simplification yields the SFG models in Fig. 10. Also note that for $a = 1$, the equivalent resistance (16) is reduced to

$$r = r_0 + Dr_1 + D'r_2. \qquad (23)$$

V. Application Guidelines and Examples

A. Application Guidelines

The proposed TIS-SFG approach is rather flexible and allows modeling of a variety of PWM converters with different configurations of coupled inductors including: switch-to-tap, diode-to-tap, rail-to-tap with isolated, cumulative or differential windings [26], as well as traditional PWM converters with simple

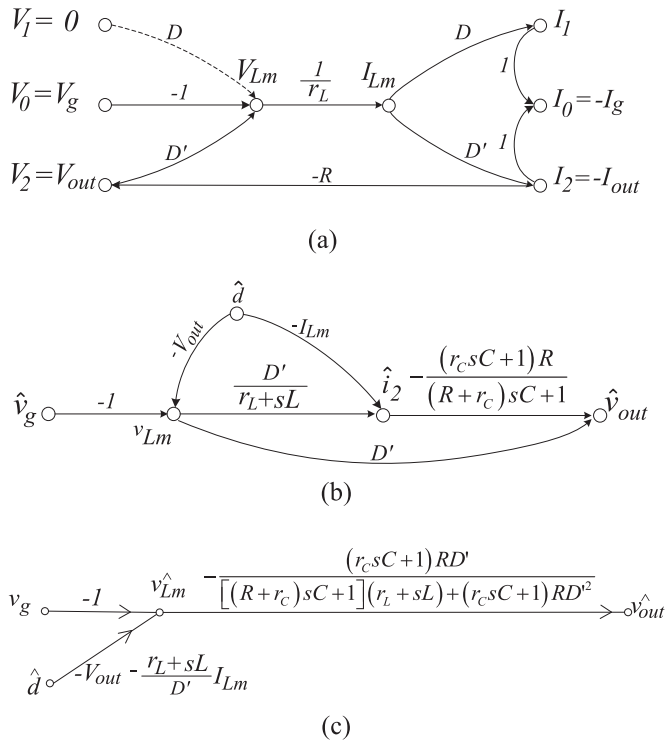

Fig. 17. SFG models of a basic boost converter including the effects of parasitic resistances r_L and r_C: (a) steady-state model; (b) small-signal model; (c) simplified small-signal model.

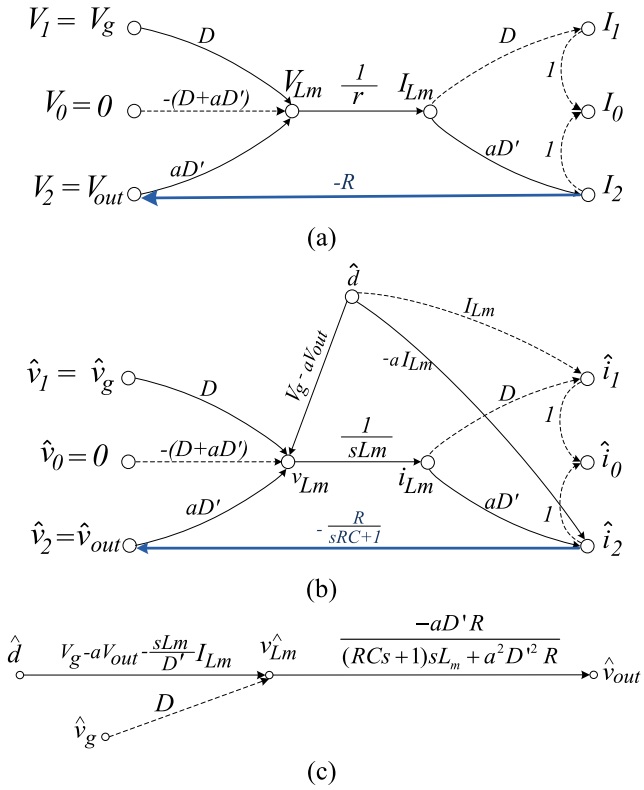

Fig. 18. SFG models of flyback converter: (a) steady-state model; (b) small-signal model; (c) simplified small-signal model.

inductors. The proposed method can be applied following the stepped procedure below.

1) Examine the given topology, identify the ports of the TIS according to Section II-B1 and list the operating conditions: terminal voltages and current polarity.
2) Identify the original windings N_1 and N_2 and their respective polarity and find the effective number of turns N_{10} and N_{20} according to Section II-B2.
3) Find the parameters of the TIS according to Sections II-B3 and B4: the magnetizing inductance L_m and the winding ratio a. Use (17) to obtain the equivalent parasitic resistance r.
4) Apply the steady-state TIS model in Fig. 8 for TI converters [for standard PWM converters, use Fig. 10(a)] to construct the steady-state SFG model of the given converter. Simplify the graph using block diagram algebra.
5) Obtain the steady-state solution.
6) Apply the small-signal TIS model in Fig. 9 [for standard PWM converters, use Fig. 10(b)] to construct the small-signal SFG model of the given converter. Simplify the graph using block diagram algebra.
7) Derive the desired small-signal transfer functions.

Examples, comparison to previous results, and verification of TIS-SFG method are presented next.

B. Modeling the TI-Boost Converter

The TI-boost topology with cumulative windings is illustrated in Table I(e). The TI-boost converter can be modeled by proper application of the derived SFG models as demonstrated next. First, the TIS module terminals can be identified as shown in Fig. 7(a). According to Section II-B1, for the TI-boost case, the terminal voltages are $v_0 = v_g$, $v_1 = 0$ also considering the designated polarity of i_2 terminal current $v_{\text{out}} = v_2 = -\frac{R}{1+sRC} i_2$. Also, since the TI boost in Table I(e) uses cumulative windings arrangement hence, $a = 1/(1+n)$.

1) Steady-State Model of the TI Boost: The steady-state model of TI boost can be attained introducing the voltage conditions above into the SFG in Fig. 8. Some branches of the initial model dashed in Fig. 11(a) are of no interest can be disregarded. Compared with the steady-state TIS model in Fig. 8, only one extra branch *–R* is added here [see the bold (blue) line in Fig. 11(a)], which represents the dependence of the output voltage V_{out} on the terminal current I_2 provided to the output by the TI. The simplified steady-state SFG is shown in Fig. 11(b). This allows finding the steady-state conditions needed to quantify the gains of various paths of the small-signal TIS model.

The desired steady-state solution of the model in Fig. 11 is straightforward. Since an ideal case is considered here, the expression is taken to the limit $r \to 0$

$$\frac{I_{Lm}}{V_g} = \lim_{r->0} -(D+aD')\frac{\frac{1}{r}}{1+\frac{a^2D'^2R}{r}} = -\frac{D+aD'}{a^2D'^2R} \quad (24)$$

and considering the current polarity definition

$$V_{\text{out}} = -I_{Lm}aD'R. \quad (25)$$

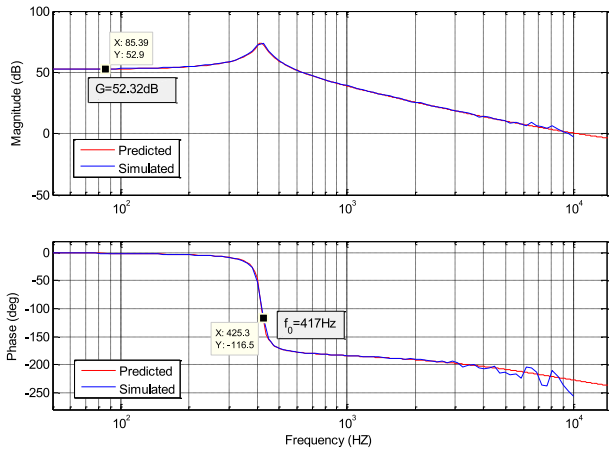

Fig. 19. Comparison of the calculated versus simulated control-to-output frequency response $\hat{v}_{\rm out}/\hat{d}$ of flyback converter ($D = 0.56$, $N = 2$, $R_{\rm load} = 200\ \Omega$, $V_O = 200$ V, $V_g = 40$ V, $L_m = 504\ \mu$f, $C_o = 47\ \mu$f, $f_S = 50$ kHz).

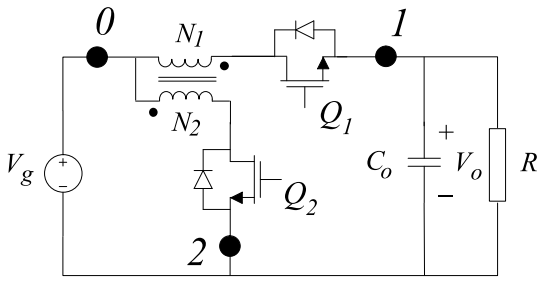

Fig. 20. WJ converter with bidirectional switches.

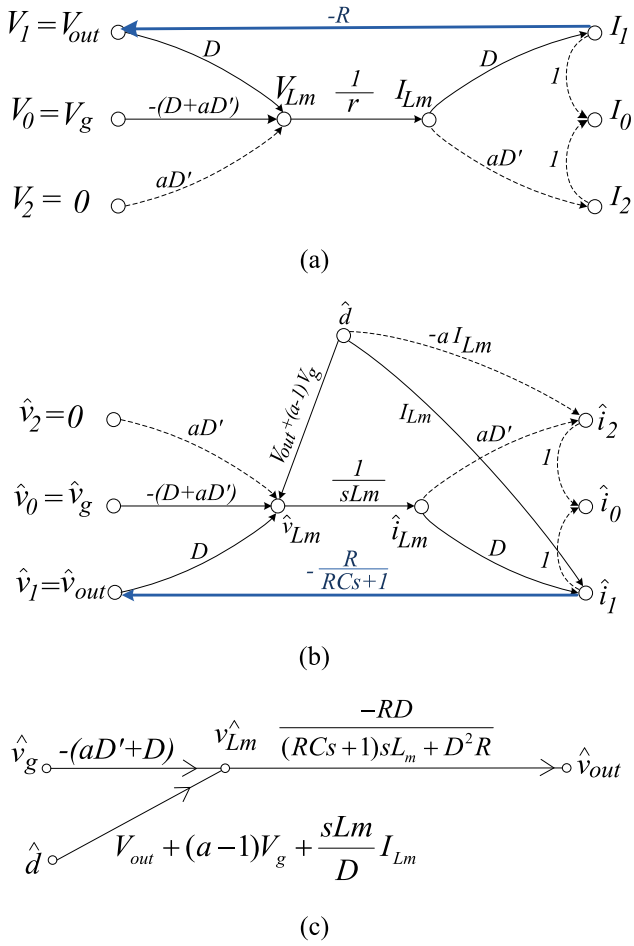

Fig. 21. SFG models of WJ converter: (a) steady-state model; (b) small-signal model; (c) simplified small-signal model.

Substituting (25) into (24), yields

$$\frac{V_{\rm out}}{V_g} = \frac{D + aD'}{aD'} = \frac{1 + nD}{D'}. \tag{26}$$

This result is identical to that reported in [27].

2) Dynamic Model of an Ideal TI Boost: The small-signal SFG of an ideal TI boost can now be obtained substituting the stated above TI's terminals conditions $V_1 = 0$, $V_0 = V_g$ and the solution obtained for the output voltage and the magnetizing current (24) into the SFG in Fig. 9. This yields SFG as shown in Fig. 12(a). Here the branches that are of no interest were removed. Also, the branches of the *d* node have been moved to the same node $\hat{v}_{Lm}$ and the closed loop between node $\hat{v}_{Lm}$ and $\hat{v}_{\rm out}$ has been simplified by graph transformation rules. Finally, the small-signal SFG model of the TI boost is obtained, as shown in Fig. 12(b).

The desired small-signal transfer functions can be easily obtained of the SFG in Fig. 12(b) as

$$\frac{\hat{v}_{\rm out}}{\hat{d}} = \frac{-aD'R}{(RCs+1)sL_m + a^2D'^2R} \times \left[(a-1)V_g - aV_{\rm out} - \frac{sL_m}{D'}I_{Lm}\right]. \tag{27}$$

Defining $L = \frac{a^2}{L_m}$ and substituting (4), (24), (25), and (26) into (27) yields

$$\frac{\hat{v}_{\rm out}}{\hat{d}} = \frac{V_{\rm out}\left[\frac{(n+1)D'}{(1+nD)} - \frac{sL}{RD'}\right]}{LCs^2 + \frac{L}{R}s + D'^2}. \tag{28}$$

Equation (28) can be further rewritten into the standard normalized form as

$$\frac{\hat{v}_{\rm out}}{\hat{d}} = \frac{G\left(1 + \frac{s}{\omega_Z}\right)}{1 + \frac{s}{Q\omega_0} + \left(\frac{s}{\omega_0}\right)^2} \tag{29}$$

where

$$G = V_g(1+n)/D'^2, \qquad \omega_Z = -\frac{(n+1)D'^2}{(1+nD)}\frac{R}{L},$$

$$\omega_0 = \frac{D'}{\sqrt{LC}}, \qquad Q = D'R\sqrt{\frac{C}{L}}.$$

This result is identical to that reported in [28].

Assuming that the converter under study operates with the following parameters: $D = 0.56$, $n = 2$, $R = 200$ Ohm, $V_O = 200$ V, $V_g = 40$ V, $L = 504\ \mu$H, $C = 47\ \mu$F; yields

$G = 619.83\,(55.84\,\text{dB})$; $\omega_Z = -108.72$ krad/s $= -17.3$ kHz; $\omega_0 = 2.8588$ krad/s $= 455$ Hz; $Q = 26.873$. The frequency response plot of the derived control to output transfer function (29) obtained by MATLAB is illustrated in Fig. 13 and was verified by PSIM simulation (see Fig. 14). Excellent matching is found.

C. Modeling the Basic Boost Converter

1) Ideal case: The small-signal transfer function of an ideal basic boost converter in Table I(b) can be derived applying the model in Fig. 10 and following the procedure outlined above. However, an alternative short-cut approach can be attempted.

As described above in Section II, for basic converters with an ordinary inductor, the winding ratio a equals unity. Hence, simply substituting $a = 1$ into the already developed TI-boost model in Fig. 11 yields the static model of the basic boost converter, as shown in Fig. 15(a). The steady-state solution is

$$\frac{I_{Lm}}{V_g} = -\frac{\frac{1}{r}}{1+\frac{D'^2R}{r}} = -\frac{1}{r+D'^2R} \underset{r->0}{=} -\frac{1}{D'^2R} \tag{30}$$

$$\frac{V_{\text{out}}}{V_g} = \frac{RD'}{r+D'^2R} \underset{r->0}{=} \frac{1}{D'}. \tag{31}$$

Similarly, the small-signal model of an ideal boost converter can be obtained by applying the condition $a = 1$ to the TI-boost small-signal model in Fig. 12. The result, as shown in Fig. 17(b), can be used to derive the small-signal transfer function

$$\frac{\hat{v}_{\text{out}}}{\hat{d}} = \frac{V_{\text{out}}\left[\frac{D'}{(1+D)} - \frac{sL}{RD'}\right]}{LCs^2 + \frac{L}{R}s + D'^2}. \tag{32}$$

2) Nonideal Case: More accurate small-signal model of the boost converter can be obtained considering the series resistance r_L of the inductor L and the equivalent series resistance (ESR) r_c of the filter capacitor C (see Fig. 16). In this example, other nonidealities are neglected. Hence, according to (23), $r = r_L$. Also note that due to current polarity convention defined in Fig. 2: $i_g = -i_0$ and $i_{\text{out}} = -i_2$.

The transfer function of the capacitive filter considering ESR is given by

$$\frac{v_2}{i_2} = -\left(r_c + \frac{1}{sC}\right)//R = -\frac{(sr_CC+1)R}{s(R+r_C)C+1}. \tag{33}$$

Here, the negative sign is due to current polarity convention according to Fig. 2.

Applying the condition $a = 1$, introducing the terminal conditions $V_1 = 0$, $V_0 = V_g$, $V_2 = V_{\text{out}}$, and considering (33), the model in Fig. 10 can be transformed into Fig. 17 and used to model the basic boost converter. Recall that the application of the model requires preliminary knowledge of the steady-state conditions derived earlier in (30) and (31).

For instance, the steady-state model can help in estimating the efficiency of the boost converter. Examining Fig. 17, it can be found that $I_g = -(D+D')I_{Lm} = -I_{Lm}$ and $I_{\text{out}} = -D'I_{Lm}$ also using (31) yields

$$\eta = \frac{V_{\text{out}}I_{\text{out}}}{V_gI_g} = \left(\frac{V_{\text{out}}}{V_g}\right)\left(\frac{I_{\text{out}}}{I_g}\right) = \left(\frac{RD'}{r_L+D'^2R}\right)\left(\frac{-D'I_{Lm}}{-I_{Lm}}\right) = \frac{1}{1+\frac{r_L}{D'^2R}}. \tag{34}$$

The obtained result (34) is identical to [29].

From Fig. 17, the input-to-output transfer function can be easily derived as

$$\frac{\hat{v}_{\text{out}}}{\hat{v}_g} = \left(\frac{D'^2R}{D'^2R+r_L}\right) \times \frac{1+r_CsC}{\frac{(R+r_C)LC}{D'^2R+r_L}s^2 + \left(Cr_C + \frac{CRr_L+L}{D'^2R+r_L}\right)s + 1}. \tag{35}$$

Equation (35) can be rewritten into the standard normalized form as

$$\frac{\hat{v}_{\text{out}}}{\hat{v}_g} = G_V\frac{\left(1+\frac{s}{\omega_z}\right)}{1+\frac{s}{Q\omega_0}+\left(\frac{s}{\omega_0}\right)^2} \tag{36}$$

where

$$G_V = \frac{D'R}{D'^2R+r_L}, \quad \omega_Z = \frac{1}{Cr_C},$$

$$\omega_0 = \sqrt{\frac{D'^2R+r_L}{R+r_C}}\frac{1}{\sqrt{LC}}, \; Q = \frac{1}{\omega_0}\left(Cr_C + \frac{CRr_L+L}{D'^2R+r_L}\right)^{-1}.$$

The control-to-output transfer function can be also obtained from Fig. 17

$$\frac{\hat{v}_{\text{out}}}{\hat{d}} = \frac{V_g}{D'}\left(\frac{D'^2R-r_L}{D'^2R+r_L}\right)\left(1-\frac{L}{D'^2R-r_L}s\right) \frac{G_V\left(1+\frac{s}{\omega_z}\right)}{1+\frac{s}{Q\omega_0}+\left(\frac{s}{\omega_0}\right)^2}. \tag{37}$$

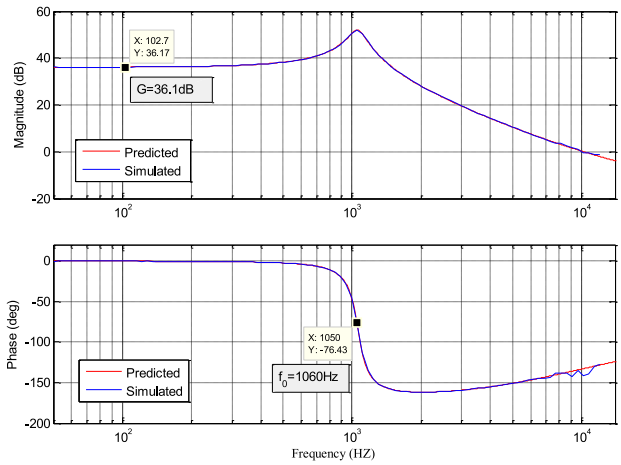

Fig. 22. Comparison of the calculated versus simulated control-to-output frequency response $\hat{v}_{\text{out}}/\hat{d}$ of WJ converter in Fig. 20(e) ($D = 0.56$, $N = 2$, $R = 20\,\Omega$, $V_O = 200$ V, $V_g = 40$ V, $L_m = 150\,\mu$f, $C_o = 47\,\mu$f, $f_S = 50$ kHz).

Equation (37) can be rewritten into the standard normalized form as

$$\frac{\hat{v}_{\rm out}}{\hat{d}} = G_d \frac{\left(1-\frac{s}{\omega_a}\right)\left(1+\frac{s}{\omega_z}\right)}{1+\frac{s}{Q\omega_0}+\left(\frac{s}{\omega_0}\right)^2} \tag{38}$$

where $G_d = \frac{D'R}{D'^2R+r_L}\frac{V_g}{D'}\left(\frac{D'^2R-r_L}{D'^2R+r_L}\right)$ and $\omega_a = \frac{D'^2R-r_L}{L}$.

The resulting transfer functions (36) and (38) are identical to earlier findings reported by [6]. The presented comparison confirms that the proposed methodology is a viable analysis approach of ordinary PWM converters.

D. Modeling the Flyback Converter

The flyback converter is a particular case of TI buck–boost converter with isolation. Since isolation has no effect on converter's transfer functions, the analysis can be performed on its equivalent nonisolated version, as shown in Table I(l). The ports of the TIS can be identified using Fig. 2 as reference and according to (4) $a = -1/n$.

Examining the circuit reveals that the operating conditions of the TIS are: $V_1 = V_g$, $V_0 = 0$, and $V_2 = V_{\rm out}$. Applying the derived earlier TIS-SFG models (see Figs. 8 and 9) and considering the output filter and load configuration, the steady state and dynamic models of flyback converter can be constructed, as shown in Fig. 18.

Analysis of the steady-state model in Fig. 18(a) yields

$$V_{\rm out} = \frac{nD}{D'}V_g \tag{39}$$

$$I_{Lm} = \frac{nV_{\rm out}}{D'R}. \tag{40}$$

The result is identical to [29].

The dynamic model in Fig. 18(b) can be simplified, as shown in Fig. 18(c). The operating point data, (39), (40), was used to identify the gains of various paths in the small-signal model.

Analysis of Fig. 18(c) yields the control to output transfer function

$$\frac{\hat{v}_{\rm out}}{\hat{d}} = \frac{G\left(1+\frac{s}{\omega_Z}\right)}{1+\frac{s}{Q\omega_0}+\left(\frac{s}{\omega_0}\right)^2} \tag{41}$$

where $G = \frac{nV_g}{D'^2}$, $\omega_0 = \frac{D'}{\sqrt{LC}}$, $Q = D'R\sqrt{\frac{C}{L}}$, $\omega_z = -\frac{D'^2}{D}\frac{R}{L}$, $L = n^2L_m$.

Assuming that the converter under study operates with the following parameters: $D = 0.56$, $n = 2$, $R = 100\ \Omega$, $V_O = 100$V, $V_g = 40$V, $L_m = 150\,\mu$H, $C = 47\,\mu$F; yields $G = 413.223(52.324$dB$)$, $\omega_Z = -57.62$ krad/s ($f_z = 9.17$ kHz), $\omega_0 = 2.62$ krad/s ($f_0 = 417$ Hz), $Q = 12.315$.

Comparison of the theoretical results predicted by (41) and PSIM simulation is shown in Fig. 19. Excellent agreement was found.

E. Modeling the Watkins–Johnson (WJ) Converter

WJ converter is an example of the rail-to-tap topology with cumulatively wound TI. Its buck, boost, and buck–boost versions can be recognized in Table I(j), (k), and (l), respectively, [24], [25]. A variant of the converter with bidirectional switches is illustrated in Fig. 20. Here, terminals of the TIS are identified. The bidirectional switches allow generating bipolar output voltage and assure CCM mode of operation. The duty cycle signal d is applied to Q_1 switch, whereas its complement d' to the Q_2. According to (4), the winding ratio of WJ converter is identical to flyback case, $a = -1/n$. Examining Fig. 20 reveals that the operating conditions of the TIS are: $V_0 = V_g$, $V_1 = V_{\rm out} = -Ri_1$, $V_2 = 0$, $i_g = -i_0$, $i_{\rm out} = -i_1$.

Applying the derived TIS-SFG models in Figs. 8 and 9, and considering the output filter and load configuration, the steady state and dynamic models of WJ converter can be constructed, as shown in Fig. 21.

Analysis of the steady-state model in Fig. 21(a) yields

$$V_{\rm out} = \left(1-\frac{D'}{nD}\right)V_g \tag{42}$$

$$I_{Lm} = -\frac{V_{\rm out}}{DR}. \tag{43}$$

According to (42), depends on the duty cycle D, the converter can generate either positive or negative output voltage. For the $n = 1$ case, the voltage conversion ratio (42) becomes identical to [29].

The dynamic model in Fig. 21(b) can be simplified as shown in (c). The operating point data, (42), (43), was used to identify the gains of various paths in the small-signal model. Analysis of Fig. 21(c) yields the control to output transfer function

$$\frac{\hat{v}_{\rm out}}{\hat{d}} = \frac{G\left(1+\frac{s}{\omega_Z}\right)}{1+\frac{s}{Q\omega_0}+\left(\frac{s}{\omega_0}\right)^2} \tag{44}$$

where $G = \frac{V_g}{nD^2}$, $\omega_0 = \frac{D}{\sqrt{L_m C}}$, $Q = DR\sqrt{\frac{C}{L_m}}$, $\omega_z = \frac{RD^2}{(nD-D')L_m}$.

Assuming that the converter under study operates with the following parameters: $D = 0.56$, $n = 2$, $R = 20\ \Omega$, $V_O = 24$ V, $V_g = 40$ V, $L_m = 150\ \mu$H, $C = 47\ \mu$F; yields $G = 63.78$ (36.1 dB), $\omega_Z = 61.49$ krad/s, $f_Z = 9.786$ kHz, $\omega_0 = 6.67$ [krad/s] ($f_0 =$1.06 kHz), $Q = 6.269$.

Comparison of the theoretical results predicted by (44) and PSIM simulation is shown in Fig. 22. Excellent agreement was found.

VI. Conclusion

Earlier SFG modeling approach has introduced the idea of a switched branch to the theory of the signal flow graph. Applying the switched branch models allowed constructing the average converter's SFG model through additional manipulation and simplification of the initial graph. Although general, the earlier approach suggested treating each converter as a new case and deriving its model "from ground up." The primary difficulty

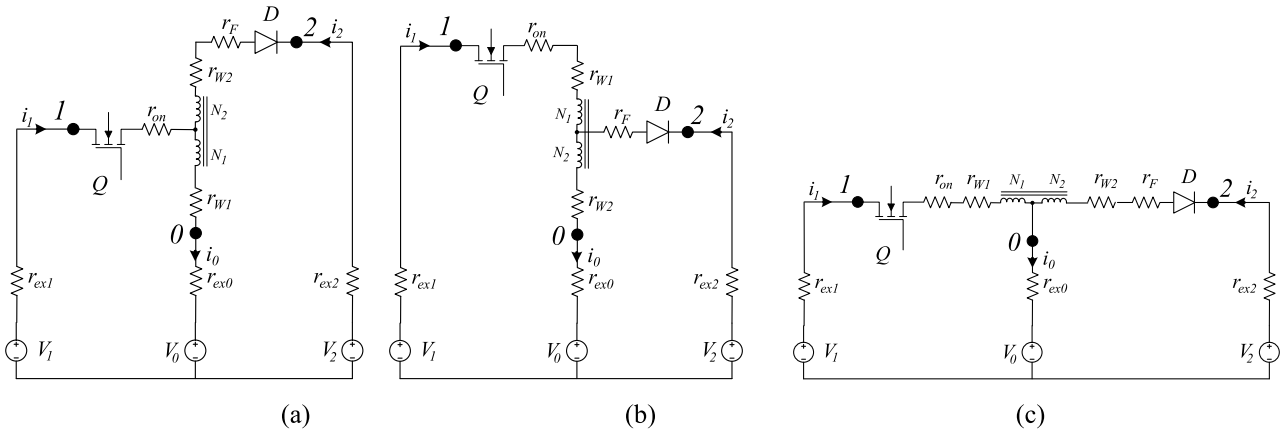

Fig. 23. Illustration of resistive components associated with the basic TI configurations: (a) switch-to-tap; (b) diode-to-tap; (c) rail-to-tap.

TABLE II
SUMMARY OF TERMINAL RESISTANCES OF BASIC TI CIRCUITS.

	Switch to tap	Diode to tap	Rail to tap
r_0	$r_{W1} + r_{ex0}$	$r_{W2} + r_{ex0}$	r_{ex0}
r_1	$r_{\rm on} + r_{ex1}$	$r_{W1} + r_{\rm on} + r_{ex1}$	$r_{W1} + r_{on} + r_{ex1}$
r_2	$r_{W2} + r_F + r_{ex2}$	$r_F + r_{ex2}$	$r_{W2} + r_F + r_{ex2}$

of the earlier methodology is the manipulation of the switched branch—a concept unfamiliar to most practicing engineers.

The advantage of SFG approach as the analysis tool is in its pictorial nature. Thus, the SFG approach was adopted in this paper. The proposed modified SFG method suggests constructing the complete flow graph model of the power stage by identifying the tapped inductor switcher, the TIS block, and applying its prefabricated equivalent and invariant TIS-SFG model as a subgraph, similarly to equivalent circuit approach. Hence, the main modeling difficulty of the earlier approach—dealing with the switched branches—is bypassed and a generalized and unified method suited for broad range of applications arises. This paper presented derivation of the steady-state and small-signal SFG models of a generalized TIS and demonstrated their application to modeling regular and TI switching converters.

To verify the proposed TIS-SFG method, several examples were presented. The results obtained with TIS-SFG model were identical to simulation and earlier theoretical results. Thus, the accuracy of the approach was confirmed. For these reasons, the proposed TIS-SFG methodology emerges as straightforward and expeditious yet, general and accurate. The proposed method emerges as a viable analysis tool that greatly alleviates the analytical effort and considerably simplifies the task of dynamic modeling of switching converters.

The proposed TIS-SFG approach is particularly well suited for theoretical study. Due to its generality and graphical nature, the TIS-SFG approach is also an easy to master educational tool. In fact, SFG methodology was applied in practice and proved to be appropriate for teaching the subject of dynamics of PWM converters as a part of the curricula of "Industrial and Power Electronics" courses suggested to undergraduate and graduate students at the University of California, Irvine.

APPENDIX

The origin of the TIS terminal resistances r_0, r_1, and r_2 in Fig. 7(a) can be clarified with reference to Fig. 23. Here, three original switches to tap, diode-to-tap, and rail-to-tap configurations of the TIs are illustrated with no consideration to winding polarity. In Fig. 23, $r_{\rm on}$ is the switch on-state resistance, r_F is the diode on-state resistance, r_{W1} is the primary's winding resistance, r_{W2} is the secondary's winding resistance, and the r_{ex0}, r_{ex1}, r_{ex2} represent the source internal resistances possibly including the series stray wiring resistance. ESR of filter capacitors of either input or output are considered as parts of filter transfer functions and are not included in $r_{ex0,1,2}$.

TIS terminal resistances can be identified and calculated as follows: r_0 is the equivalent resistance through which the charging current i_1 and the discharging current i_2 flow through. The terminal resistance r_1 is the equivalent resistance through which only i_1 flows, and r_2 is the equivalent resistance through which only i_2 flows. Table II summarizes the terminal resistances of the example circuits in Fig. 23. Note that the isolated coupled inductor circuits, e.g., flyback converter, have no common tap and, therefore, $r_0 = 0$.

REFERENCES

[1] R. D. Middlebrook, "Small-signal modeling of pulse-width modulated switched-mode power converters," *Proc. IEEE*, vol. 76, no. 4, pp. 343–354, Apr. 1988.
[2] R. B. Ridley, "A new, continuous-time model for current-mode control," *IEEE Trans. Power Electron.*, vol. 6, no. 2, pp. 271–280, Apr. 1991.
[3] F. D. Tan and R. D. Middlebrook, "A unified model for current-programmed converters," *IEEE Trans. Power Electron.*, vol. 10, no. 4, pp. 397–408, Jul. 1995.
[4] R. D. Middlebrook, "Predicting modulator phase lag in PWM converter feedback loops," in *Proc. 8th Int. Solid-State Power Convers. Conf.*, Apr. 1981, pp. H4.1–H4.6.
[5] R. D. Middlebrook and S. Cuk, *Advances in Switched-Mode Power Conversion*, vols. I–III. Pasadena, CA, USA: TESLAco, 1983.
[6] G. W. Wester and R. D. Middlebrook, "Low-frequency characterization of switched dc-dc converters," *IEEE Trans. Aerosp. Electron. Syst.*, vol. AES-9, no. 3, pp. 376–385, May 1973.
[7] R. D. Middlebrook and S. C'uk, "A general unified approach to modeling switching-converter power stages," in *Proc. IEEE Power Electron. Spec. Conf.*, 1976, pp 18–34.

[8] W. M. Polivka, P. R. K. Chetty, and R. D. Middlebrook, "State space average modeling of converters with parasitics and storage-time," in *Proc. IEEE Power Electron. Spec. Conf. Rec.*, 1980, pp. 119–143.
[9] S.-P. Hsu, A. Brown, L. Rensink, and R. D. Middlebrook, "Modeling and analysis of switching dc-to-dc converters in constant-frequency current-programmed mode," in *Proc. IEEE Power Electron. Spec. Conf. Rec.*, 1979, pp. 284–301.
[10] R. D. Middlebrook, "Topics in multiple-loop regulators and current-mode programming," *IEEE Trans. Power Electron.*, vol. PE-2, no. 2, pp. 109–124, Apr. 1987.
[11] M. Clique and J. Fossard, "A general model for switching converters," *IEEE Trans. Aerosp. Electron. Syst.*, vol. AES-13, no. 4, pp. 397–400, Jul. 1977.
[12] P. R. K. Chetty, "Current injected equivalent circuit approach to modeling switching DC-DC converters," *IEEE Trans. Aerosp. Electron. Syst.*, vol. AES-17, no. 6, pp. 802–808, Nov. 1981.
[13] A. R. Brown and R. D. Middlebrook, "Sampled-data modeling of switched regulators," in *Proc. Power Electron. Spec. Conf. Rec.*, 1981, pp. 349–369.
[14] F. C. Y. Lee and Y. Yu, "Computer-aided analysis and simulation of switched dc-dc converters," *IEEE Trans. Ind. Appl.*, vol. IA-15, no. 5, pp. 511–520, Sep. 1979.
[15] G. C. Verghese, C. A. Bruzos, and K. N. Mahabir, "Averaged and sampled-data models for current mode: A reexamination," in *Proc. Power Electron. Spec. Conf. Rec.*, 1989, pp. 484–491.
[16] K. Smedley and S. Cuk, "Switching flow-graph nonlinear modeling technique," *IEEE Trans. Power Electron.*, vol. 9, no. 4, pp. 405–413, Jul. 1994.
[17] S. Ben-Yaakov, "SPICE simulation of PWM DC-DC converter systems: Voltage feedback, continuous inductor conduction mode," *Electron. Lett.*, vol. 25, no. 16, pp. 1061–1063, Aug. 1989.
[18] Y. Amran, E. Huliehel, and S. Ben-Yaakov, "A unified SPICE compatible average model of PWM converters," *IEEE Trans. Power Electron.*, vol. 6, no. 4, pp. 585–594, Oct. 1991.
[19] A. Abramovitz, "An approach to average modeling and simulation of switch-mode systems," *IEEE Trans. Educ.*, vol. 54, no. 3, pp. 509–517, Aug. 2011.
[20] A. Pietkiewicz and D. Tollik, "Unified topological modeling method of switching DC-DC converters in duty-ratio programmed mode," *IEEE Trans. Power Electron.*, vol. PE-2, no. 3, pp. 218–226, Jul. 1987.
[21] V. Vorperian, "Simplified analysis of PWM converters using model of PWM switch. Continuous conduction mode," *IEEE Trans. Aerosp. Electron. Syst.*, vol. 26, no. 3, pp. 490–496, May 1990.
[22] R. D. Middlebrook, "Measurement of loop gain in feedback systems," *J. Electron.*, vol. 38, no. 1, pp. 485–512, Apr. 1975.
[23] B. W. Williams, "Unified synthesis of tapped-inductor dc-to-dc converters," *IEEE Trans. Power Electron.*, vol. 29, no. 10, pp. 5370–5383, Oct. 2014.
[24] D. A. Grant and Y. Darroman, "Watkins-Johnson converter completes tapped inductor converter matrix," *Electron. Lett.*, vol. 39, pp. 271–272, Feb. 2003.
[25] T. Y. Ann, "Operation analysis of the Watkins-Johnson converter," *J. Inst. Electron. Eng. Korea S*, vol. 36-S, no. 8. pp. 113–122, 1999 (in Korean).
[26] K. W. E Cheng, "Tapped inductor for switched-mode power," in *Proc. Int. Conf. Power Electron. Syst. Appl.*, 2006, pp. 14–20.
[27] N. Vazquez, L. Estrada, C. Hernandez, and E. Rodrigue, "The tapped-inductor boost converter," in *Proc. IEEE Int. Symp. Ind. Electron.*, 2007, pp. 538–543.
[28] S. Dwari, S. Jayawant, T. Beechner, S. K. Miller, A. Mathew, M. Chen, J. Riehl, and J. Sun, "Dynamics characterization of coupled-inductor boost DC-DC converters," in *Proc. IEEE Workshop Comput. Power Electron.*, Jul. 2006, pp. 264–269.
[29] R. W. Erickson and D. Maksimovic, *Fundamentals of Power Electronics*, 2nd ed. Boston, MA, USA: Kluwer, 2001.
[30] R. Priewasser, M. Agostinelli, C. Unterrieder, S. Marsili, and M. Huemer, "Modeling, control, and implementation of DC–DC converters for variable frequency operation," *IEEE Trans. Power Electron.*, vol. 29, no. 1, pp. 287–301, Jan. 2014.
[31] M. Veerachary, T. Senjyu and K. Uezato, "Signal flow graph nonlinear modelling of interleaved converters," *IEE Proc. Electric Power Appl.*, vol. 148, no. 5, pp. 410–418, Sep. 2001.
[32] P. C. Loh, D. M. Vilathgamuwa, C. J. Gajanayake, Y. R. Lim, and C. W. Teo, "Transient modeling and analysis of pulse-width modulated z-source inverter," *IEEE Trans. Power Electron.*, vol. 22, no. 2, pp. 498–507, Mar. 2007.
[33] Li-C. Liao, C.-T. Pan, and T.-L. Jong, "Switching flow-graph modeling technique for three-phase inverters," *IEEE Trans. Ind. Electron.*, vol. 55, no. 4, pp. 1603–1613, Apr. 2008.
[34] M. Veerachary, "Analysis of fourth-order dc–dc converters: A flow graph approach," *IEEE Trans. Ind. Electron.*, vol. 33, no. 1, pp. 133–141, Jan. 2008.
[35] M. Zhu and F. Lin Luo, "Enhanced self-lift CUK converter for negative-to-positive voltage conversion," *IEEE Trans. Power Electron. Lett.*, vol. 25, no. 9, pp. 2227–2233, Sep. 2010.
[36] C. Zheng, L. Su, and D. Ma, "A systematic USFG design approach for integrated reconfigurable switched-capacitor power converters," *IEEE Trans. Circuits Syst.*, vol. 58, no. 11, pp. 2790–2800, Nov. 2011.
[37] Z. Zhang, C. Ole Thomsen, and A. E. Michael Andersen, "Modeling and control of a dual-input isolated full-bridge boost converter," in *Proc. Appl. Power Electron. Conf. Expo.*, Feb. 2012, pp. 2017–2023.

Authors' photographs and biographies not available at the time of publication.